HHS Public Access

Author manuscript

Hear Res. Author manuscript; available in PMC 2016 September 01.

Published in final edited form as:

Hear Res. 2015 September ; 327: 163–174. doi:10.1016/j.heares.2015.06.007.

Morphological Correlates of Hearing Loss after Cochlear Implantation and Electro-Acoustic Stimulation in a Hearing-Impaired Guinea Pig Model

Lina A.J. Reiss[1], **Gemaine Stark**[1], **Anh T. Nguyen-Huynh**[1], **Kayce A. Spear**[1], **Hongzheng Zhang**[1,2], **Chiemi Tanaka**[1,3], and **Hongzhe Li**[1]

[1] Oregon Hearing Research Center, Department of Otolaryngology, Oregon Health & Science University, 3181 SW Sam Jackson Park Road, Portland, OR 97239, USA

[2] Department of Otolaryngology Head & Neck Surgery, Zhujiang Hospital of Southern Medical University, Guangzhou 510280, China

[3] Department of Communication Sciences and Disorders, John A. Burns School of Medicine, University of Hawai'i at Mānoa, 677 Ala Moana Blvd, Honolulu, HI 96816, USA

Abstract

Hybrid or electro-acoustic stimulation (EAS) cochlear implants (CIs) are designed to provide high-frequency electric hearing together with residual low-frequency acoustic hearing. However, 30-50% of EAS CI recipients lose residual hearing after implantation. The objective of this study was to determine the mechanisms of EAS-induced hearing loss in an animal model with high-frequency hearing loss.

Guinea pigs were exposed to 24 hours of noise (12-24 kHz at 116 dB) to induce a high-frequency hearing loss. After recovery, two groups of animals were implanted (n=6 per group), with one group receiving chronic acoustic and electric stimulation for 10 weeks, and the other group receiving no stimulation during this time frame. A third group (n=6) was not implanted, but received chronic acoustic stimulation. Auditory brainstem responses were recorded biweekly to monitor changes in hearing. The organ of Corti was immunolabeled with phalloidin, anti-CtBP2, and anti-GluR2 to quantify hair cells, ribbons and post-synaptic receptors. The lateral wall was immunolabeled with phalloidin and lectin to quantify stria vascularis capillary diameters. Bimodal or trimodal diameter distributions were observed; the number and location of peaks were objectively determined using the Aikake Information Criterion and Expectation Maximization algorithm.

Noise exposure led to immediate hearing loss at 16-32 kHz for all groups. Cochlear implantation led to additional hearing loss at 4-8 kHz; this hearing loss was negatively and positively correlated with minimum and maximum peaks of the bimodal or trimodal distributions of stria vascularis capillary diameters, respectively. After chronic stimulation, no significant group changes in

Corresponding Author: Lina A.J. Reiss, Ph.D., Oregon Hearing Research Center, Department of Otolaryngology, Oregon Health and Science University, 3181 SW Sam Jackson Park Road, Portland, OR 97239, Phone: (503) 494-2917, Fax: (503) 494-5656, reiss@ohsu.edu.

Conflict of Interest

The authors declare that we have no conflict of interest.

thresholds were seen; however, elevated thresholds at 1 kHz in implanted, stimulated animals were significantly correlated with decreased presynaptic ribbon and postsynaptic receptor counts. Inner and outer hair cell counts did not differ between groups and were not correlated with threshold shifts at any frequency.

As in the previous study in a normal-hearing model, stria vascularis capillary changes were associated with immediate hearing loss after implantation, while little to no hair cell loss was observed even in cochlear regions with threshold shifts as large as 40-50 dB. These findings again support a role of lateral wall blood flow changes, rather than hair cell loss, in hearing loss after surgical trauma, and implicate the endocochlear potential as a factor in implantation-induced hearing loss. Further, the analysis of the hair cell ribbons and post-synaptic receptors suggest that delayed hearing loss may be linked to synapse or peripheral nerve loss due to stimulation excitotoxicity or inflammation. Further research is needed to separate these potential mechanisms of delayed hearing loss.

Keywords

Hybrid; cochlear implant; electro-acoustic stimulation; stria vascularis; synapse; hearing loss

1. Introduction

The goal of Hybrid or electro-acoustic stimulation (EAS) cochlear implants (CIs) is to provide high-frequency electric hearing while preserving residual low-frequency acoustic hearing for combined electric and acoustic stimulation in the same ear. The Hybrid or EAS CI is a shorter, thinner version of the traditional CI, and is implanted using soft surgery techniques which include careful, slow insertion of the electrode into the cochlea (Kiefer et al., 2002; Gantz and Turner, 2003). This type of CI is aimed for patients with a severe-profound high-frequency hearing loss, but good low-frequency hearing, who would not be candidates for a traditional full-length CI.

The advantages of using EAS over using a traditional CI alone include superior speech recognition in the presence of background talkers (Turner et al., 2004; Dorman et al., 2008), superior musical melody and instrument recognition (Gfeller et al., 2006, Dorman et al., 2008), and improved ability to use localization cues to attend to a speaker in spatially separated noise (Gifford et al., 2013; Rader et al., 2013). Further, speech perception outcomes are superior when hearing is preserved even when the CI is used alone without the acoustic hearing, i.e. without acoustic amplification; this indicates the importance of minimizing the damage to neurosensory structures for effective electrical stimulation (Carlson et al., 2011; Fitzpatrick et al., 2014).

However, between 30-55% of EAS CI patients lose 30 dB or more of their residual low-frequency hearing within months after implantation (Gantz et al., 2009; Gstoettner et al., 2009; Santa Maria et al., 2013). The hearing loss does not typically occur right after surgery, but is slow and may take several months to manifest. While many EAS CI patients can function well on speech recognition in quiet with the electric CI component alone, they lose the additional benefits of EAS for speech recognition in noise, as well as for musical melody

discrimination and sound localization (Gantz et al., 2009). Clearly, hearing preservation success rates need to be improved in order to allow full benefit from EAS.

The mechanism underlying this residual hearing loss is unknown. Retrospective analysis of subject risk factors in the Hybrid clinical trial indicate increased risk of implant-induced hearing loss with male gender, age, and an etiology of noise-induced hearing loss (Kopelovich et al., 2014). Studies in animal models are conflicting; some studies suggest that an inflammatory or immune response to electrode insertion trauma can lead to hair cell death (Eshraghi et al., 2013), while other studies have shown that this hearing loss is not explained by hair cell or spiral ganglion cell loss (Tanaka et al., 2014; O'Leary et al., 2013). Other proposed factors, such as fibrosis or bone growth, show weak correlations with hearing loss and are unlikely to play a major role in hearing loss after cochlear implantation (Tanaka et al., 2014; O'Leary et al., 2013).

In our previous study, we tested an alternative hypothesis, that electro-acoustic stimulation itself may cause hearing loss (Tanaka et al., 2014). Guinea pigs were implanted for up to 3 months, and hearing preservation and histology were compared in animals that were stimulated versus two sets of controls, implanted animals without stimulation and non-implanted animals. We were able to replicate both a high-frequency hearing loss immediately after surgery and a delayed low-frequency hearing loss in the stimulated group several weeks after implantation. The only histological changes associated with hearing loss were increased cross-sectional area and decreased blood vessel or capillary density of the stria vascularis (SV), the part of the cochlear lateral wall responsible for maintaining the high endocochlear potential or “battery” required for hair cells to transduce sound. This finding is consistent with a proposed role of the lateral wall in implantation trauma due to its vulnerable location in the path of the electrode insertion (Wright and Roland, 2013). However, this association was limited to the high-frequency hearing loss. The delayed low-frequency hearing loss was not explained by changes viewable under a light microscope, such as hair cell, spiral ganglion cell, or stria vascularis changes, or by fibrosis or ossification.

The previous findings suggest that the low-frequency hearing loss may instead be caused by more subtle changes, such as at the hair cell synapse, rather than hair cell death. Previous studies have shown glutamate excitotoxicity occurs after noise-induced hearing loss and can be mimicked by glutamate agonists (e.g. Pujol et al., 1985; Puel et al., 1994; Wang and Green, 2011). Further, such excitotoxicity can eventually lead to irreversible loss of the hair cell synapses and nerve fibers, even after “temporary” hearing loss (Kujawa and Liberman, 2009; Lin et al., 2011; Wang and Green, 2011), The clinical association of post-implantation hearing loss with an etiology of noise-induced hearing loss also suggests a possible excitotoxic mechanism that would only be visible in the hair cell synapses or nerve fibers (Kopelovich et al., 2014).

Another caveat is that normal-hearing animals were used in the previous study. It is possible that pre-existing hearing loss or sub-threshold damage may influence the effects of EAS on residual hearing. Thus, in this study, we extended the investigation of EAS effects on hearing to guinea pigs with high-frequency, noise-induced hearing loss similar to that in EAS CI

patients, and used immunolabeling of both ribbon synapses and post-synaptic receptors to determine whether changes at the hair cell synapse could explain the delayed EAS-induced low-frequency hearing loss. Immunolabeling of SV vasculature was also used to further examine the relationship between SV capillary diameters and high-frequency hearing loss, and rule out a contribution of SV vasculature changes to delayed low-frequency hearing loss.

2. Materials and Methods

2.1 Subjects

Sixteen male, 4-week old albino Dunkin-Hartley guinea pigs were purchased from Charles River Laboratories (Wilmington, MA). All animal protocols were approved by the Oregon Health & Science University Committee on the Use and Care of Animals and veterinary care was provided by the Department of Comparative Medicine (IACUC#IS00000672).

2.2 Research Design

All animals were exposed to 24 hours of octave-band noise (12-24 kHz) at 116 dB to induce a high-frequency hearing loss in the frequency regions to be stimulated by the electrode array, as in human Hybrid CI patients. Animals were allowed to recover for at least 4 weeks to allow sufficient time for recovery from temporary threshold shifts (Miller et al., 1963). After recovery, animals were divided into three groups: 1) non-implanted Chronic Acoustic Stimulation controls (CAS; n=6, 4 non-implanted animals, 6 ears; for 2 animals, both ears were used); 2) implanted No Stimulation controls (NS; n=6); and 3) implanted Chronic Acoustic and Electric Stimulation animals (CAES; n=6). The CAS group consisted of non-implanted guinea pigs that received chronic acoustic stimulation. The other two groups underwent cochlear implant surgery at 5 weeks after the noise exposure. The NS group underwent cochlear implantation, but received no direct acoustic or electric stimulation. The CAES group underwent cochlear implantation and received chronic combined acoustic and electric stimulation.

Starting 8 weeks after noise exposure (3 weeks after cochlear implantation), CAES and CAS animals were stimulated 3 hours/day, 5 days/week for 9.5 weeks with modulated white noise while they were restrained. NS animals were restrained for the same amount of time, but with no stimulation. Auditory brainstem responses (ABRs) were recorded to monitor changes in hearing. Animals were sacrificed at the conclusion of the stimulation period (18 weeks after noise exposure) and cochleae were collected for histological analysis.

2.3 Cochlear implants

Standard 8-ring animal electrode arrays with a ball electrode (#Z60275, Cochlear Limited, Lane Cove, Australia) were used in the current study. These electrode arrays were chosen because they have the same chemical composition and assembly as the clinical CI electrodes. Five to seven of the electrodes were inserted into the scala tympani.

The diameter of the implant was 0.45 mm, and the centers of the electrodes were 0.75 mm apart. An encased receptacle with an attached electrode was fastened to the top of the skull with 3 medical-grade stainless steel screws. Three medical-grade stainless steel brackets

with screw holes were attached to the receptacle for skull attachment. All electrode array assemblies were chemically sterilized using ethylene oxide before implantation.

2.4 Surgical Procedures for Implanted Animals

For all implanted animals, the CI surgery was performed on the left ear. The animals were anesthetized with ketamine (60 mg/kg) and xylazine (5 mg/kg) through intramuscular (IM) injection. Supplemental doses of anesthetics were given as necessary. The surgical area was shaved and aseptically prepared with 70% ethanol and Betadine. Local anesthesia (lidocaine 2 mg/kg) was injected subcutaneously (SC) along the intended incisions. The subjects were placed on a heating pad and rectal temperature was maintained around 36 °C. In addition to the temperature, vital signs (heart rate, respiratory rate, oxygen level, and pulse rate) were recorded using a vital signs monitor.

Surgery was performed as follows under a surgical microscope. Through a left postauricular incision, the left bulla was exposed and opened using a 1.4 mm acorn burr and rongeur to gain access to the round window niche. Through a midline skull incision, the CI connector was secured to top of the skull with three screws and with methyl methacrylate. The CI electrode array and ball electrode were tunneled along the skull underneath soft tissue into the left bulla. The ball electrode was then positioned under the left temporalis muscle. A cochleostomy was made just inferior and anterior to the round window using a 0.5 mm diamond burr. Through the cochleostomy, the CI electrode array was slowly inserted into the scala tympani until slight resistance was felt. Between five to seven electrodes were inserted and the number of intracochlear electrodes was recorded for each animal [See Suppl. Fig. 1 for images of typical electrode insertions in two cochleae]. Based on the cochleostomy location, insertion angle, and insertion depth, the frequencies stimulated at the tip of the electrode in the cochlea were estimated to vary between 12-16 kHz (Greenwood, 1990). The cochleostomy was sealed with muscle plugs.

During this surgery, the right ear was mechanically deafened to prevent bone-conduction cross-hearing effects from the non-implanted ear on ABR threshold estimates from the CI side. Deafening was induced by opening the round window and the basal turn of cochlea of the right ear and thorough suctioning of perilymph, which was found in previous studies to be more effective and reliable than boring a sharp object into the cochlea, as well as minimizing vestibular side effects (Tanaka et al., 2014). This deafening procedure was only used for implanted animals.

Upon completion of the skin closure, electrode impedance was measured using Cochlear Custom Sound software. Postoperatively, chloramphenicol sodium succinate (30 mg/kg, IM), buprenorphine (0.05 mg/kg, SC), and 10-ml warmed lactated ringers (SC) were given. Vitamin C (10 mg/kg, IM), meloxicam (0.2 mg/kg, oral), silver sulfadiazine cream (1%, topical) and 10-ml warmed lactated ringers (SC) were provided for three days postoperatively. Animals were kept warm and monitored until fully conscious, and allowed to recover for 2 weeks.

2.5 Auditory Brainstem Response (ABR) and Electrically-Evoked Auditory Brainstem Response (EABR) Testing

All testing was conducted using Tucker-Davis Technologies hardware and software. Prior to the testing, the guinea pigs were anesthetized with IM ketamine (30 mg/kg) and xylazine (5 mg/kg) administration and placed on the heating pad inside an acoustic booth. A rectal probe was inserted to monitor body temperature and maintain it around 36 °C. Otoscopic examination was performed to check the status of the outer and middle ear. Subcutaneous needle electrodes were placed between the eyes (non-inverting), below the ipsilateral pinna near the cheek (inverting), and below the contralateral pinna near the cheek (ground).

ABRs were conducted before noise exposure, 4 weeks after noise exposure, and before the conclusion of the study in all animals. Additional ABRs were conducted in implanted animals in 2-week intervals beginning at 2 weeks after surgery up to the end of the study. Test stimuli consisted of tone bursts at 1, 2, 4, 8, and 16 kHz (5 ms duration, 1 ms rise/fall time with Cos2 gating, 21 stimulus/sec, alternating), as well as 32 kHz before and after noise exposure. The speaker was placed 10 cm from the ipsilateral auditory meatus and contralateral ear was plugged with a silicon earplug. The animals' evoked responses were amplified with a gain of 5,000 and band-pass filtered from 100 Hz – 3 kHz using a Signal Recovery Model 5113 preamplifier. Responses to 300 sweeps were averaged at each stimulus level. The level of the testing signal was initially decreased in 10-dB steps from 90 dB SPL, and then in 5-dB steps to search for the threshold, defined as the lowest level at which a detectable Wave III response was elicited and repeated.

EABRs were recorded in implanted animals in 2-week intervals beginning at 2 weeks after implantation up to the end of the study. Impedance testing was performed before each session to ensure that electrodes were not open or shorted. Custom Sound EP software and external CI components (programming pod, refurbished Freedom speech processor, and implant emulator, and custom-made CI cable) were used to measure impedances and deliver electrical stimulation to the CI. The same electrode montage and recording parameters were used as for ABR. Using the ball electrode as a ground (Monopolar 1), 300 responses to testing electrical signals (49 pulse per sec, 25 μs pulse width, 8 μs inter pulse gap, alternating current, −200 μs delay) were averaged. The electric current level was either increased or decreased in 10-CL steps (current level in microamperes (μA) on a log scale similar to dB (5.7 CL = 1 dB)) from 100 CL initially, and then 5-CL steps to search for the EABR threshold, defined as the lowest current level at which a detectable Wave II or III response was elicited and repeated.

2.6 Cochlear Implant Programming

The CIs in the CAES group were programmed at 3 weeks after implantation using the same external components as for EABR and clinical Custom Sound. The animals were placed inside a custom-made restraint tube (Snyder and Salvi, 1994) during programming. The Freedom speech processor was set to use monopolar stimulation (ball electrode as a ground), the Advanced Combination Encoder (ACE) processing strategy with 6 maxima (essentially chronic interleaved sampling (CIS)), 1200 pulses per second, and a 25 μs pulse width. Frequency table 6 was used to allocate the frequency range of 188 – 7938 Hz to the

electrode array. Impedance testing was performed before setting T- and C- levels (minimum and maximum levels), and only functioning electrodes with measurable impedances (i.e. not open-circuit) were turned on. EABR thresholds were used to set T-levels, and C-levels were determined based on behavioral responses such as pinna twitching, vocalization, agitation, and teeth chattering. These behaviors were observed to make sure that the C-levels did not cause discomfort to the animals. Muscle artifacts such as pinna/whisker twitching or head movements synchronous with pulse train stimulation sometimes occurred, indicating cranial nerve stimulation and limiting the maximum stimulation levels that could be used. The CI map was created by Custom Sound software and written to the speech processor. C-levels were measured and adjusted weekly to maximize the dynamic range, as is done in the clinic, and T-levels were set according to biweekly EABR measures.

2.7 Chronic Stimulation

Chronic stimulation procedures were similar to those in the previous study (Tanaka et al., 2014). Chronic stimulation for the CAES and CAS groups was conducted in a double-walled sound-treated booth. All animals were placed inside a custom-made restraint tube that was modified for guinea pigs (Snyder and Salvi, 1994). Up to 6 animals with restraint tubes were placed on the table in a circle. The loudspeaker was placed 37 cm above the surface of the table in the center of the circle. Amplitude modulated white noise (50% amplitude modulation depth, 60 dBA, 30 Hz) was generated using MATLAB, and was used as a stimulus since it can stimulate a broad frequency range and because modulated noise is dynamic, like speech. The stimulus was presented through Microsoft Windows Player using a desktop computer and delivered simultaneously through the loudspeaker for the acoustic stimulation for both CAS and CAES animals, and an amplifier with direct audio input (DAI) connection to a Freedom speech processor for the electrical stimulation for the CAES animals only. For CAES animals, the Freedom speech processor was connected to the animal via an implant emulator and custom cable connection to the CI receptacle on the animal's head; the processor microphone was disabled to only allow DAI. The implant emulator converted the signal from the speech processor into biphasic pulse trains exactly like those provided clinically (25 μs pulse width, 8 μs inter pulse gap). The final mean T-and C-levels averaged across all 6 electrodes for each animal varied from 23 μA (NE-18) to 272 μA (NE-7) and 185 μA (NE-17) to 282 μA (NE-7), respectively, with overall group mean T-level of 162 μA and group mean C-level of 235 μA. The final mean dynamic range across all electrodes for each animal varied from 10 μA (NE-7) to 258 μA (NE-18), with a group mean dynamic range of 73 μA. Electric thresholds (T-levels) were significantly correlated with ABR threshold shifts in the electrode region at 16 kHz for this group ($R=0.93$; $p=0.007$), consistent with a previous study that showed that acoustic threshold shifts lead to elevated electric thresholds (Kang et al, 2010).

The level of the amplitude modulated white noise was set at 60 dBA ± 1 dB at the animal's ear level using a Brüel &Kjær sound level meter with a 1 inch microphone. This presentation level was used since it did not cause temporary or permanent threshold shift in normal-hearing guinea pigs in a pilot study.

2.8 Histology

After 9.5 weeks and final ABR/EABR measurements, all animals were euthanized with an overdose of a ketamine-xylazine combination, and perfused intracardially with saline followed by fixative (4% paraformaldehyde). The cochleae were collected and decalcified in 10% EDTA for 7-10 days. Once decalcified, the electrode array was removed and the cochleae were microdissected into ~11 pieces and organ of Corti and lateral wall sections were immunostained separately for confocal imaging.

Organ of Corti sections were triple-labeled as shown in Figure 1, first with primary antibodies directed against a synaptic ribbon protein (Figure 1B; mouse IgG1 anti-CtBP2, BD Transduction Labs; 1:50), and a post-synaptic receptor protein (Figure 1C; mouse IgG2a anti-GluR2, Millipore; 1:500). A merging of the two labels is shown in Figure 1D, and Figure 1E is an enlarged version of the box outlined in Figure 1D that illustrates the overlap of the red ribbon protein and green post-synaptic receptor protein labels. After primary incubation, secondary antibodies were added: goat anti-mouse IgG1 AF568 (Invitrogen; 1:1000), goat anti-mouse IgG2a AF488 (Invitrogen; 1:1000), and phalloidin AF647 (Figure 1A; Invitrogen; 1:250). Lateral wall sections were labeled with fluorescein-labeled lectin (Vector Laboratories, Burlingame, CA; 1:100) to reveal capillary structures, and additionally counter-labeled with Alexa Fluor-647 phalloidin (Life Technologies, Carlsbad, CA: 1:250).

Both organ of Corti and lateral wall sections were then whole-mounted in Vecta Shield (Vector Laboratories, Burlingame, CA) and observed using a Nikon Eclipse TE300 inverted confocal microscope. Fluorescence emission was collected sequentially. Confocal imaging was used to image organ of Corti sections at 1 μm intervals and lateral wall sections at 4 μm intervals.

2.9 Histological analysis

For organ of Corti sections, hair cells were counted using the phalloidin stain, and ribbons and post-synaptic receptors were counted using the double label. Missing hair cells were identified by the characteristic X-shaped phalangeal scar on the cuticular lamina (Fig. 1A; Raphael and Altschuler, 1991). The scar is of Deiter's cell-origin, forming an adherens junction line between 2 scarring Deiter's cells (Anttonen et al., 2012). Ribbon and post-synaptic receptor counts were restricted to those within complete hair cells in the image, and normalized by the number of hair cells. Each inner hair cell body was identified by the aggregation of a cluster of anti-CtBP2 (and anti-GlutR2) labeling (Fig. 1B-D). Anti-CtBP2 also labels the nucleus of surviving hair cells, providing a convenient reference for each cluster of synaptic structures (Fig. 1B). The longitudinal distance along the organ of Corti used to assess hair cell numbers (or synaptic counts) for each frequency location was 1024 pixels * 0.262 micron = 268 micron, or 0.27 mm. For correlation analyses with ABR thresholds, histology analysis of the organ of Corti focused on sections corresponding to the 1, 2, 4, and 8 kHz regions.

For the lateral wall sections, stria vascularis capillary widths were measured using the phalloidin and lectin stains. Histology analyses of the lateral wall focused on the 1.5 kHz and 6 kHz regions. We selected these frequency regions because the morphological

examination at 1, 2, 4, and 8 kHz was initially prioritized towards synapse measurement, and thus this tissue was not available for the stria vascularis analysis. Alternative cochlear segments if available, or in some circumstances, the residue tissue from synapse measures, were further processed to evaluate the capillary diameter. Random samples of capillary width were taken using ImageJ, with up to 45 measurements per image and distributed on all branches (Fig. 2A). Example distributions of capillary width indicated unimodal distributions (Fig. 2B), as well as bimodal distributions in many cases (Fig. 2C,D), and the occasional trimodal distribution (Fig. 2E,F). These examples indicated the necessity of objectively determining 1) whether the distribution was unimodal, bimodal, or even possibly trimodal; 2) the locations of the peak(s). The Aikake Information Criterion (AIC), a well-known information-theoretic measure of how well a model fits a given distribution, was computed to assess whether the distribution was best fit by a unimodal, bimodal, or trimodal Gaussian mixture distribution model (McLachlan and Peel, 2000). The model that produced the minimum AIC indicated which model best fit the data (example values for each model shown in Fig. 2B-F). If the unimodal distribution had the smallest AIC, i.e. the distribution was determined to be unimodal, the mean of the distribution was estimated as the single peak. If the bimodal or trimodal distribution had the smallest AIC, an iterative algorithm called Expectation Maximization was run to calculate the mean value of each peak in the distribution (Dempster et al., 1977; example curve fitting results are shown in Fig. 2B-F). The first peak was classified as the baseline peak, corresponding to baseline capillary widths in the absence of dilation. The highest peak (the second peak in a bimodal distribution, or the third peak in a trimodal distribution) was classified as the maximum peak, which presumably corresponds to capillary widths at maximum dilation. The MATLAB Statistical Toolbox (Mathworks, Inc., Natick, MA) was used to calculate AIC and run the Expectation Maximization algorithm.

3. Results

3.1 Acoustic ABR threshold shifts after noise exposure, implantation, and stimulation

Figure 3 shows changes in acoustic ABR thresholds as a function of frequency after each procedure – noise exposure, cochlear implantation, and chronic electro-acoustic stimulation.

All three groups of animals were exposed to noise that led to a steeply sloping high-frequency hearing loss limited to 16 and 32 kHz at 4 weeks after noise exposure (three curves in Fig. 3A), i.e. in the vicinity of the noise exposure band (gray region in Fig. 3A). A within/between subjects ANOVA showed significant effects for frequency ($p<10^{-27}$), but not group.

Within 2 weeks after cochlear implantation, both CAES and NS implanted groups had significant additional threshold shifts, referenced to thresholds at 4 weeks after the noise exposure; a within/between subjects ANOVA of the CAES and NS groups showed significant effects again of frequency, but not group, indicating that both groups had similar threshold shift patterns after surgery ($p<10^{-8)}$. Pairwise analyses indicated that the CAES group had significantly greater threshold shift than the CAS group at 8 kHz (p=0.045) and the NS group had significantly greater threshold shifts than the CAS group at 4 kHz (p=0.043) and 8 kHz (p=0.001). The non-implanted control CAS group is not shown here

because no surgery was performed on that group. Note that unlike the previous study in normal-hearing animals (Tanaka et al., 2014), there was no additional implant-induced hearing loss at 16 kHz due to the pre-existing hearing loss at 16 kHz induced by the noise exposure.

After 9.5 weeks of chronic electro-acoustic stimulation for the CAES group, the CAES group showed an additional mean threshold shift of 8 dB at 1 kHz, referenced to thresholds at 2 weeks after cochlear implantation green circles, Fig. 3C; also compare distributions shown in detail in Fig. 3D,F); however, a within/between ANOVA revealed no effects of group or frequency and this threshold shift was not quite significantly different from the mean threshold shift of -3 dB in the non-implanted CAS group ($p=0.066$) or the threshold shift of 2 dB in the NS group ($p>0.1$). No correlations were observed between the individual CAES group threshold shifts and maximum current levels or dynamic ranges of stimulation.

3.2 Inner and outer hair cell counts

No significant differences in inner or outer hair cell counts were seen between groups at any frequency up to the 8 kHz region($p>0.05$, between/within subjects ANOVA), consistent with the previous study (Tanaka et al., 2014). For reference, the 8 kHz region is equivalent to 12.1 mm from the apex, or 6.4 mm from the base for an 18.5 mm long cochlea (Greenwood, 1990). Figure 4 shows the group averaged hair cell survival percentages for each section or frequency, and Table I shows the raw surviving and total hair cell counts, with survival percentages in bold. Outer hair cells are shown in Fig. 4A, and inner hair cells are shown in Fig. 4B. Different colors and symbols indicate the different groups. Typically the total raw number of hair cells counted for each frequency region ranged between 25-30 inner hair cells and 90-110 outer hair cells per cochlea; average hair cell counts per cochlea are given in Table 1.

Correlation analyses further showed no correlations of inner or outer hair cell counts with ABR thresholds at any frequency ($p>0.05$, Pearson correlation test; not shown).

3.3 Ribbon and post-synaptic receptor counts

Figure 5 shows the group-averaged ribbon and post-synaptic counts for each section or frequency. Pre-synaptic ribbon counts are shown in Fig. 5A, and post-synaptic receptor counts are shown in Fig. 5B.

Pre-synaptic ribbon group mean counts ranged from 11.7-18.1 ribbons per cell. Significant effects of frequency, but not group were observed ($p<10^{-10}$, between/within subjects ANOVA). Post-hoc analysis indicated that all the frequency regions differed significantly from each other, except for 4 kHz versus 8 kHz ($p<0.05$, two-tailed t-test with Bonferroni correction). Examination of Figure 5A suggests a trend in which the number of pre-synaptic ribbons generally increases from 1 kHz to 4 kHz, i.e. from low to high frequencies. Post-synaptic receptor counts were lower, with group mean counts ranging from 7.5-12.7 receptors per cell. Similar to ribbon counts, receptor counts showed significant effects of frequency, but not group ($p=0.02$, between/within subjects ANOVA).

However, group averaged analyses do not account for the variability in threshold changes within groups. Scatter plots in Figure 6 indicate significant negative correlations of synapse count with final ABR thresholds at 1 kHz for both pre-synaptic ribbons and post-synaptic receptors. Despite the small sample size, these correlations are significant for ribbon counts in the CAES group (R= -0.81, p=0.049, Pearson correlation test; green circles in Fig. 6A), but not quite significant for receptor counts (R= −0.80, p=0.054; green circles and fitted line in Fig. 6E). Correlations are also significant at 1 kHz when ribbon counts are pooled across CAES, NS, and CAS groups (R= −0.48, p=0.013; black lines in Fig. 6A). Similarly, correlations are significant when receptor counts are pooled across groups at 1and 2 kHz (R= − 0.65, p=0.004 and R= −0.51, p=0.031, respectively; black lines in Fig. 6E, 6F). Note that all of these correlations are negative and have negative R values. There is also a not-quite significant positive correlation of receptor count with ABR thresholds at 8 kHz for the CAES group (R=+0.94, p=0.056, Pearson correlation test; green circles in Fig. 6H).

Interestingly, while trends were not significant within the NS group, a negative trend with thresholds is suggested at 1, 2, and 4 kHz (red triangles in Fig. 6A-C, E-G).

Scatter plots of pre-synaptic ribbon counts versus post-synaptic receptor counts in individual animals are shown in Figure 7. Significant correlations were observed for the CAES group at 1 kHz and for pooled data at 2 kHz only ($p<0.05$, Pearson two-tailed correlation test; green circles and fitted line in Fig. 7A and black line in Fig. 7B). For the CAES group, the slope of the fit was 3.7, which means that there were 3.7 ribbons for every receptor. Note that for all frequencies and groups, receptor counts were generally below the dotted line relative to ribbon counts.

3.4 Baseline and maximum dilation widths of capillaries in the stria vascularis

Initial comparisons of overall mean SV capillary diameters indicated no significant differences between groups, nor were there correlations with ABR thresholds. However, when discrete peaks were calculated for bimodal or trimodal distributions, both minimum and maximum peak widths of SV capillaries at the 6 kHz region showed significant correlations with ABR thresholds. Correlations were conducted with ABR thresholds at 4 kHz and 8 kHz, due to lack of threshold data for 6 kHz. Figure 8A shows that the minimum peak in the distributions of SV capillary widths, i.e. the first peak in Fig. 2B, was significantly negatively correlated with threshold at 8 kHz (R=−0.71, p=0.028). An almost significant correlation was also seen with 4 kHz (R=−0.64, p=0.053). Figure 8B shows that the maximum peak in the distributions of capillary widths, i.e. the second peak in Fig. 2B when two peaks were present or the baseline peak when only one peak was present, was significantly positively correlated with threshold at 8 kHz (R=0.73, p=0.018). A significant positive correlation was also seen versus 4 kHz thresholds (R=0.78, p=0.008, not shown). This correlation is due to the presence of multimodal distributions for animals with more hearing loss.

No significant correlations were seen between SV capillary minimum or maximum peak widths at the 1.5 kHz region with ABR thresholds at 1 or 2 kHz (not shown). However, a significant difference was seen in maximum peak widths between the CAES and CAS

groups for this frequency region (p=0.028, t-test), i.e. the CAS group had a larger maximum peak diameter of 15.7 μm than the 12.6 μm peak diameter of the CAES group.

No correlations were seen between SV capillary widths and either pre-synaptic ribbon or post-synaptic receptor counts at either frequency region.

4. Discussion

4.1 Hearing-impaired guinea pig model of hearing loss after cochlear implantation

After 24 hours of exposure to a 12-24 kHz noise at 116 dB, a consistent high-frequency hearing loss was produced in all animals. The threshold shifts occurred in a limited frequency range of 16 and 32 kHz, as desired, reproducing the steeply sloping high-frequency hearing loss of typical Hybrid or EAS CI recipients. Moreover, this model is consistent with a noise-induced hearing loss etiology seen in many Hybrid CI users, especially those who experienced hearing loss after cochlear implantation (Kopelovich et al., 2014).

The implanted hearing-impaired guinea pig model also experienced similar hearing loss trends as the previous normal-hearing model (Tanaka et al., 2014). All implanted animals experienced a high-frequency hearing loss immediately after implantation, mainly at 4 and 8 kHz, since hearing loss was already maximized at 16 and 32 kHz from the noise exposure. It should be noted that the 4 and 8 kHz frequency regions are quite apical to the electrode insertion, which at a maximum of 5 mm insertion depth would go no deeper than 12 kHz (Greenwood, 1990). These threshold shifts apical to the electrode insertion have also been reported in previous studies (e.g. Kang et al., 2010; O'Leary et al., 2013; Tanaka et al., 2014).

After 9.5 weeks of electro-acoustic stimulation, chronically stimulated animals experienced an additional small delayed low-frequency hearing loss at 1 kHz; however, this threshold shift was not significantly different from the non-implanted or implanted controls. Thus, it is not yet clear whether the delayed hearing loss at 1 kHz was due to the chronic electro-acoustic stimulation, or from general inflammation arising from implantation itself. Certainly, a number of previous studies did not find long-term effects of electric stimulation on hearing thresholds (Coco et al., 2007; Ni et al., 1992; Shepherd et al., 1983; Xu et al., 1997); these studies contrast with those that found neurite damage with electric stimulation (Kopelovich et al., 2015). However, it should be noted that the former studies used electric stimulation only without concurrent acoustic stimulation. Due to the small effect sizes, future experiments with longer daily stimulation over a longer implantation period are needed to rule out hearing loss due to electro-acoustic stimulation, as well as separate effects due to electro-acoustic stimulation versus general inflammatory processes, as no anti-inflammatory agents were used in this study.

4.2 Inner and outer cell counts show no effect of implantation or stimulation

Inner and outer hair cell counts did not differ between implanted and non-implanted animals, and were uncorrelated with hearing loss at any frequency, up to 8 kHz. Above 8 kHz in the noise exposure frequency band, more outer hair cell loss and/or overall damage was

observed; for instance, of four animals also quantified at 12 kHz, one had complete outer hair cell loss, consistent with studies of hair cell loss after high-level noise exposure (e.g. Hamermik et al., 1989; Choudhury et al., 2011). The lack of association of hair cell counts with implantation-induced hearing loss below the noise band replicate some previous studies looking at effects of implantation (Tanaka et al., 2014; O'Leary et al., 2013; Kang et al., 2010) and chronic stimulation (Tanaka et al., 2014; Coco et al., 2007), but are not consistent with others which found extensive hair cell loss in implanted animals (Eshraghi et al., 2013). One likely reason for the discrepancy is the difference in the degree of hearing loss induced by electrode insertion trauma; the former studies induced less trauma and hearing loss than the latter study. More severe trauma could lead to more widespread damage in the cochlea, including but not limited to hair cells. Note that this is in contrast to the initial 80-90% post-operative hearing preservation rate when a skilled surgeon uses soft surgery techniques (Gantz et al., 2009; Gstoettner et al., 2009; Santa Maria et al., 2013); thus, broad damage and hair cell loss with severe electrode insertion trauma may obscure other potential mechanisms that may be more important in implantation-induced hearing loss encountered clinically.

4.3 Reduced ribbon and receptor counts are associated with low-frequency hearing loss

One of the goals of this study was to examine other, more subtle factors besides hair cell loss, such as synaptic changes, which might explain the delayed low-frequency hearing loss. For 1, 2, and 4 kHz, we did not find any group average differences in inner hair cell pre-synaptic ribbon counts or post-synaptic receptor counts. However, it is important to note that there was significant variation in both hearing loss and ribbon counts *within* the two implanted experimental groups, likely due to the variability in surgical trauma across individuals. Thus, the more important measure may be how threshold variations are associated with ribbon count variations across individuals in the group, i.e. a correlation analysis.

When correlation analyses were used, both ribbons and receptor counts showed negative correlations with thresholds, i.e. the poorer the threshold, the lower the ribbon or receptor count. This correlation was significant for the ribbon counts within the implanted, stimulated CAES group at 1 kHz. The correlation was also significant for data when pooled across groups for ribbon counts at 1 kHz, receptor counts at 1 kHz, and receptor counts at 2 kHz. Further, it should be noted that while not significant, negative correlations were also consistently seen for the 2 and 4 kHz frequency regions for both ribbon and receptor counts.

One potential interpretation of the association of synaptic changes with hearing loss in the CAES group is that electric-only or electro-acoustic stimulation leads to excitotoxicity similar to what happens with acoustic over-stimulation in noise exposure. It is also possible that electrical stimulation inhibits the regeneration of new post-synaptic receptors, as found after noise exposure (Puel et al., 1998; Pujol and Puel, 1999), i.e. provides negative feedback in the receptor turnover system. However, a similar trend is suggested in the implanted, non-stimulated NS group, and significance increases with pooled data, suggesting an alternative interpretation that the synaptic changes may be due to inflammation or other side effects of implantation itself rather than excitotoxicity via electric or electro-acoustic stimulation. It is

also possible that with inflammation, synapses may be more vulnerable to excitotoxicity from acoustic stimulation alone. Further study is needed utilizing inflammation markers in conjunction with threshold and synaptic changes to determine this relationship.

Another, less likely possibility is that the synaptic changes may simply be a delayed effect of the noise exposure. The clustering and lack of correlations in the non-implanted CAS control group makes this interpretation less likely. Previous findings also show that after noise exposure, ribbon loss is limited to 10% at frequencies inside and below the noise band, compared to more than 50% at frequencies above the noise band (Kujawa and Liberman, 2009; Lin et al., 2011).

It is possible that at higher frequencies closer to the electrode insertion site, electrode insertion trauma can lead to reduced ribbon counts. Ribbon counts also increased with frequency up to 4 kHz, consistent with previous findings showing that synaptic density peaks in mid-frequency regions in mice and gerbils (Meyer et al., 2009; Kujawa and Liberman, 2009).

It is interesting that an almost significant positive correlation of receptor counts with ABR threshold was observed for the CAES animals at 8 kHz; one could speculate that the higher acoustic thresholds in the correlation were due to other causes than synapse loss, but at the same time these higher thresholds reduced synaptic activation and excitotoxic damage to synapses during EAS.

Post-synaptic receptor counts were generally lower than ribbon counts within the same animal, suggesting stronger effects of implantation and/or EAS on receptors and neurites than ribbons. Certainly, ribbon counts may underestimate synaptic damage, because many ribbons may no longer be connected to receptor terminals (Lin et al., 2011). In-vivo studies using electrical stimulation also suggest that stimulation selectively damages neurofilaments or causes them to retract, while leaving hair cells intact (Kopelovich et al., 2015). The more severe reduction of receptors, but not ribbons, in the CAES group compared to the NS group at 8 kHz may support this interpretation. Alternatively, noise in the background of the receptor label may have obscured receptors and led to an underestimate of receptor counts, compared to ribbon counts.

4.4 Multimodal SV capillary widths are associated with high-frequency hearing loss

As in the previous study (Tanaka et al., 2014), significant correlations were seen between SV capillary widths and thresholds. However, due to the multiple samples of capillary widths distributed over all vascular branches throughout the SV in each animal, multimodal distributions were observed instead of simply reduced overall SV capillary area as in the previous study. These multimodal distributions indicate more complex relationships of vessel widths with threshold than would have been found using a cross-sectional area measurement. The two peaks, rather than overall mean widths, were negatively and positively correlated with thresholds, respectively. In other words, smaller capillaries were narrower and larger capillaries were wider in animals with more hearing loss, i.e. there was greater separation between peaks.

Multimodal distributions do not occur commonly in normal-hearing animals, but have recently been shown to be more prevalent after cochlear insult such as via endotoxemia or noise exposure (Li et al., 2011, 2015; Koo et al., 2015), homologues of local inflammatory responses. These findings illustrate the importance of careful analysis of multiple peaks in capillary distributions rather than just mean values when multimodal distributions are present.

The lower minimum peak values (reduction in smaller capillary widths), but not the higher maximum peak values (increase in larger capillary widths) with hearing loss are consistent with the previous findings of overall reduced SV capillary area with increased hearing loss (Tanaka et al., 2014). One possible mechanism suggested by the findings is that lateral wall trauma with electrode insertion leads to collapse of smaller or branch capillaries, which in turn affects blood flow and reduces the ability of the SV to maintain the endocochlear potential. It is possible that smaller capillaries are more important functionally than larger capillaries in determining SV metabolic capacity. Alternatively, smaller capillaries may reflect reduced baseline diameters of capillaries due to lateral wall trauma, and larger capillaries may reflect increased dilation as a compensatory response to reduced baseline diameters. Prior noise exposure and/or implantation trauma may also trigger chronic inflammatory events that further alter capillary structure with to-be-determined immune and molecular mechanisms. Another possibility, which was not explored here, is that fibrosis or ossification in response to trauma may alter capillary function as well as induce a conductive loss.

5. Conclusions

In summary, the findings do not clearly point to any one mechanism of hearing loss with cochlear implantation, but rather indicate the involvement of multiple mechanisms. For hearing loss in and just apical to the electrode region, the data confirm a link to SV capillary density, but not hair cell survival. For hearing loss far apical to the electrode region, one potential mechanism is excitotoxicity and hair cell synapse loss with electro-acoustic stimulation, similar to that seen with noise exposure; alternatively, synapse loss could arise from general inflammation due to surgical trauma or the presence of the cochlear implant electrode array as a foreign body. Further research with longer stimulation durations and with characterization of inflammation markers is needed to separate these effects.

Supplementary Material

Refer to Web version on PubMed Central for supplementary material.

Acknowledgements

This study was funded by the Hearing Health Foundation (LR), NIH-NIDCD R03DC011622 (HL), and the Ed Everts Medical Student Fellowship (KS). Stimulating electrode arrays were provided by Cochlear. Additional support was provided by the NIH/NIDCD core grant P30DC005983. We thank Charles and Leslie Liberman for the CtBP2 and GluR2 labeling protocol, Steven Green and Elisabeth Glowatzki for additional advice on immunolabeling methodology and analysis, and Alfred Nuttall for helpful comments on the manuscript.

Abbreviations

ABR	Auditory brainstem response
ACE	Advanced Combination Encoder
AIC	Aikake Information Criterion
CAES	Chronic Acoustic Electric Stimulation
CAS	Chronic Acoustic Stimulation
CI	Cochlear implant
CIS	Chronic Interleaved Sampling
DAI	Direct Audio Input
EABR	Electrically-evoked auditory brainstem response
EAS	Electric and acoustic stimulation
IHC	Inner hair cell
IM	Intramuscular
NS	No stimulation
OHC	Outer hair cell
SV	Stria vascularis, stria vascular

References

Anttonen T, Kirjavainen A, Belevich I, Laos M, Richardson WD, Jokitalo E, Brakebusch C, Pirvola U. Cdc42-dependent structural development of auditory supporting cells is required for wound healing at adulthood. Sci. Rep. 2012; 2:978. [PubMed: 23248743]

Carlson ML, Driscoll CLW, Gifford RH, Service GJ, Tombers NM, Hughes-Borst BJ, Neff BA, Beatty CW. Implications of minimizing trauma during cochlear implantation. Otol. Neurootol. 2011; 32:962–968.

Choudhury B, Adunka OF, Demason CE, Ahmad FI, Buchman CA, Fitzpatrick DC. Detection of intracochlear damage with cochlear implantation in a gerbil model of hearing loss. Otol Neurotol. 2011; 32(8):1370–8. [PubMed: 21921858]

Coco A, Epp SB, Fallon JB, Xu J, Millard RE, Shepherd RK. Does cochlear implantation and electrical stimulation affect residual hair cells and spiral ganglion neurons? Hear Res. 2007; 225:60–70. [PubMed: 17258411]

Dempster AP, Laird NM, Rubin DB. Maximum likelihood from incomplete data via the EM algorithm. J. Royal Statistical Society, Series B. 1977; 39(1):1–38.

Dorman MF, Gifford RH, Spahr AJ, McKarns SA. The benefits of combining acoustic and electric stimulation for the recognition of speech, voice and melodies. Audiol Neurootol. 2008; 13(2):105–12. [PubMed: 18057874]

Eshraghi AA, Gupta C, Van De Water TR, Bohorquez JE, Garnham C, Bas E, Talamo VM. Molecular mechanisms involved in cochlear implantation trauma and the protection of hearing and auditory sensory cells by inhibition of c-Jun-N-terminal kinase signaling. Laryngoscope. 2013; 123(Suppl 1):S1–14. [PubMed: 23382052]

Fitzpatrick DC, Campbell AT, Choudhury B, Dillon MP, Forgues M, Buchman CA, Adunka OF. Round window electrocochleography just before cochlear implantation: Relationship to word recognition outcomes in adults. Otol. Neurootol. 2014; 35:64–71.

Gantz BJ, Turner CW. Combining acoustic and electrical hearing. Laryngoscope. 2003; 113:1726–30. [PubMed: 14520097]

Gantz BJ, Hansen MR, Turner CW, Oleson JJ, Reiss LA, Parkinson AJ. Hybrid 10 clinical trial: preliminary results. Audiol. Neurootol. 2009; 14(Suppl 1):32–8. [PubMed: 19390173]

Gfeller KE, Olszewski C, Turner C, Gantz B, Oleson J. Music perception with cochlear implants and residual hearing. Audiol. Neurootol. 2006; 11(Suppl 1):12–5. [PubMed: 17063005]

Gifford RH, Dorman MF, Skarzynski H, Lorens A, Polak M, Driscoll CL, Roland P, Buchman CA. Cochlear implantation with hearing preservation yields significant benefit for speech recognition in complex listening environments. Ear Hear. 2013; 34(4):413–25. [PubMed: 23446225]

Gstoettner W, Helbig S, Settevendemie C, Baumann U, Wagenblast J, Arnoldner C. A new electrode for residual hearing preservation in cochlear implantation: first clinical results. Acta Otolaryngol. 2009; 129:372–9. [PubMed: 19140036]

Greenwood DD. A cochlear frequency-position function for several species--29 years later. J Acoust Soc Am. 1990; 87:2592–605. [PubMed: 2373794]

Hamernik RP, Patterson JH, Turrentine GA, Ahroon WA. The quantitative relation between sensory cell loss and hearing thresholds. Hear. Res. 1989; 38:199–212. [PubMed: 2708163]

Kang SY, Colesa DJ, Swiderski DL, Su GL, Raphael Y, Pfingst BE. Effects of hearing preservation on psychophysical responses to cochlear implant stimulation. J Assoc Res Otolaryngol. 2010; 11:245–65. [PubMed: 19902297]

Kiefer, J.; Tillein, J.; von Ilberg, C.; Pfennigdorff, T.; Sturzebecher, E.; Klinke, R.; Gstottner, W. Fundamental aspects and first clinical results of the clinical application of combined electric and acoustic stimulation of the auditory system.. In: Kubo, T.; Takahashi, Y.; Iwaki, T., editors. Advances in Cochlear Implants - An Update. Kugler Publications; The Hague: 2002. p. 569-576.

Koo, JW.; Quintanilla-Dieck, L.; Jiang, M.; Liu, J.; Urdang, ZD.; Li, H.; Steyger, PS. Endotoxemia-mediated Inflammation Potentiates Aminoglycoside-induced Ototoxicity, Science Translational Medicine. 2015. (conditionally accepted)

Kopelovich JC, Reiss LAJ, Etler CP, Xu L, Bertroche JT, Gantz BJ, Hansen MR. Hearing loss after activation of hearing preservation cochlear implants might be relatead to afferent cochlear innervation injury. Otol. Neurotol. 2015; 36(6):1035–44. [PubMed: 25955750]

Kopelovich JC, Reiss LA, Oleson JJ, Lundt ES, Gantz BJ, Hansen MR. Risk factors for loss of ipsilateral residual hearing after hybrid cochlear implantation. Otol. Neurotol. 2014; 35(8):1403–8. [PubMed: 24979394]

Kujawa SG, Liberman MC. Adding insult to injury: Cochlear nerve degeneration after “temporary” noise-induced hearing loss. J. Neurosci. 2009; 29(45):14077–14085. [PubMed: 19906956]

Li H, Wang Q, Steyger PS. Acoustic trauma increases cochlear and hair cell uptake of gentamycin. PLOS ONE. 2011; 6(4):e19130. [PubMed: 21552569]

Li, H.; Liu, J.; Steyger, PS. Characterizing strial capillary dilation in mouse models of sound-enhanced intra-cochlear aminoglycoside trafficking. Midwinter Research Meeting of the Association for Research in Otolaryngology; Baltimore, MD.. 2015.

Lin HW, Furman AC, Kujawa SG, Liberman MC. Primary neural degeneration in the guinea pig cochlea after reversible noise-induced threshold shift. J. Assoc. Res. Otolaryngol. 2011; 12:605–616. [PubMed: 21688060]

McLachlan, G.; Peel, D. Finite mixture models. Wiley; Hoboken, NJ: 2000.

Meyer AC, Frank T, Khimich D, Hoch G, Riedel D, Chapochnikov NM, Yarin YM, Harke B, Hell SW, Egner A, Moser T. Tuning of synapse number, structure and function in the cochlea. Nat. Neurosci. 2009; 12(4):444–53. [PubMed: 19270686]

Miller JD, Watson CS, Covell WP. Deafening effects of noise on the cat. Acta. Oto-Larynol. Suppl. 1963; 176:1–91.

Ni D, Shepherd RK, Seldon HL, Xu SA, Clark GM, Millard RE. Cochlear pathology following chronic electrical stimulation of the auditory nerve. I: Normal hearing kittens. Hear Res. 1992; 62:63–81. [PubMed: 1429252]

O'Leary SJ, Monksfield P, Kel G, Connolly T, Souter MA, Chang A, Marovic P, O'Leary JS, Richardson R, Eastwood H. Relations between cochlear histopathology and hearing loss in experimental cochlear implantation. Hear Res. 2013; 298:27–35. [PubMed: 23396095]

Pujol R, Lenoir M, Robertson D, Eybalin M, Johnstone BM. Kainic acid selectively alters auditory dendrites connected with cochlear inner hair cells. Hear. Res. 1985; 18:145–151. [PubMed: 2864329]

Puel JL, Pujol R, Tribillac F, Ladrech S, Eybalin M. Excitatory amino acid antagonists protect cochlear auditory neurons from excitotoxicity. J. Comp. Neurol. 1994; 341:241–256. [PubMed: 7512999]

Puel JL, Ruel J, Gervais D'Aldin C, Pujol R. Excitotoxicity and repair of cochlear synapses after noise-trauma induced hearing loss. Neuroreport. 1998; 9:2109–2114. [PubMed: 9674603]

Pujol R, Puel JL. Excitotoxicity, synaptic repair, and functional recovery in the mammalian cochlea: a review of recent findings. Ann. N. Y.Acad. Sci. 1999; 884:249–254. [PubMed: 10842598]

Rader T, Fastl H, Baumann U. Speech perception with combined electric-acoustic stimulation and bilateral cochlear implants in a multisource noise field. Ear Hear. 2013; 34(3):324–32. [PubMed: 23263408]

Raphael Y, Altschuler RA. Reorganization of cytoskeletal and junctional proteins during hair cell degeneration. Cell Motil. Cytoskeleton. 1991; 18(3):215–227. [PubMed: 1711932]

Santa Maria PL, Domville-Lewis C, Sucher CM, Chester-Browne R, Atlas MD. Hearing preservation surgery for cochlear implantation--hearing and quality of life after 2 years. Otol. Neurotol. 2013; 34:526–31. [PubMed: 23503094]

Shepherd RK, Clark GM, Black RC. Chronic electrical stimulation of the auditory nerve in cats. Physiological and histopathological results. Acta Otolaryngol Suppl. 1983; 399:19–31. [PubMed: 6316712]

Snyder DL, Salvi RJ. A novel chinchilla restraint device. Lab Animal. 1994; 24:42–44.

Tanaka C, Nguyen-Huynh A, Loera K, et al. Factors associated with hearing loss in a normal-hearing guinea pig model of hybrid cochlear implants. Hear. Res. 2014; 316C:82–93. [PubMed: 25128626]

Turner CW, Gantz BJ, Vidal C, Behrens A, Henry BA. Speech recognition in noise for cochlear implant listeners: benefits of residual acoustic hearing. J. Acoust. Soc. Am. 2004; 115:1729–35. [PubMed: 15101651]

Wang Q, Green SH. Functional role of NT-3 in synapse regeneration by spiral ganglion neurons on inner hair cells after excitotoxic trauma *in vitro*. J. Neurosci. 2011; 31(21):7938–7949. [PubMed: 21613508]

Wright CG, Roland PS. Vascular trauma during cochlear implantation: a contributor to residual hearing loss? Otol. Neurotol. 2013; 34:402–7. [PubMed: 23222961]

Xu J, Shepherd RK, Millard RE, Clark GM. Chronic electrical stimulation of the auditory nerve at high stimulus rates: a physiological and histopathological study. Hear Res. 1997; 105:1–29. [PubMed: 9083801]

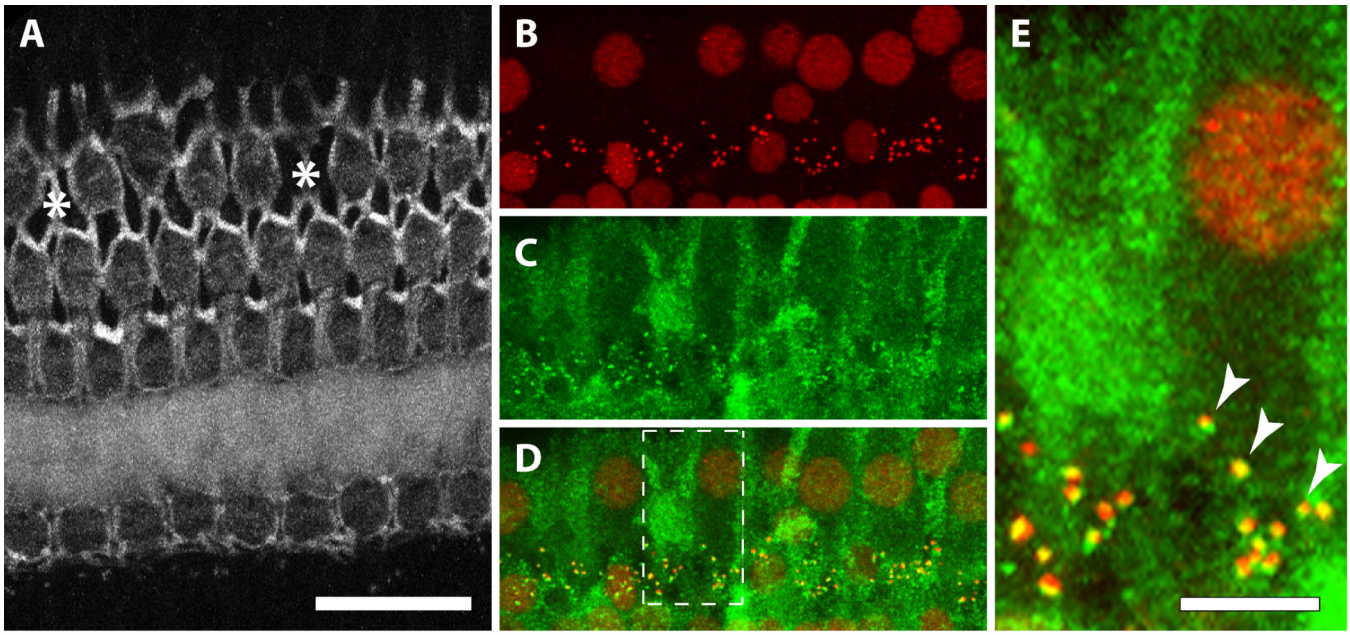

Figure 1.

Images from a cochlear segment below 1 kHz. **A.** Phalloidin-labeled cuticular plates of hair cells. Asterisks represent missing 3rd row OHCs. **B.** IHC nuclei and presynaptic ribbons both label with anti-CtBP2 (from the same cochlear segment as in A). **C.** Post-synaptic receptors and cytoplasmic background label with anti-GluR2. **D.** Merged images from B and C. Dashed lines indicate inset displayed in E. Scale bar in A is shared for A-D. **E.** Arrowheads show the co-localization of CtBP2 (red) and GluR2 (green).

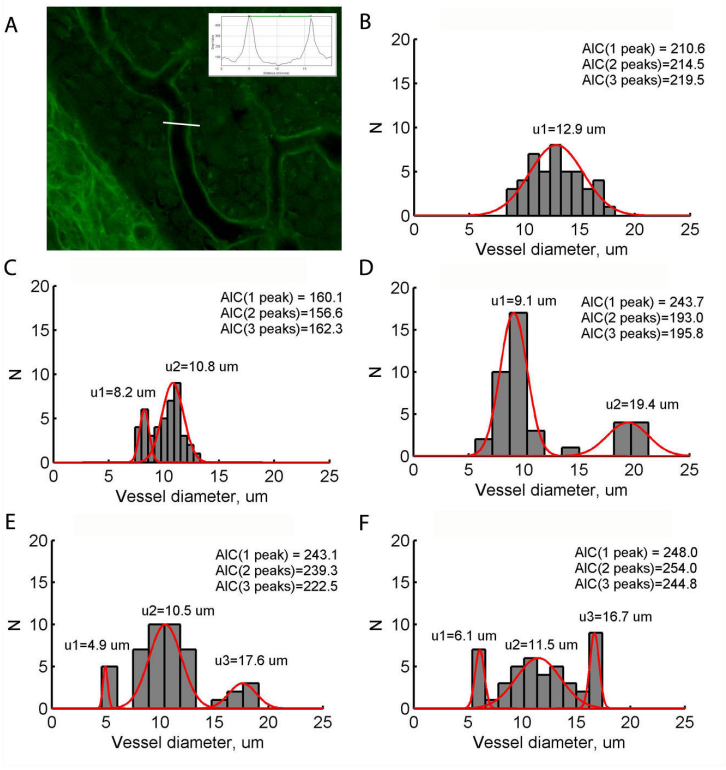

Figure 2.

Analysis of stria vascularis capillary diameters. **A.** Example image of stria vascularis labeled with fluorescein and lectin. The stria vascularis capillary widths were quantified by multiple samples of capillary diameters taken using ImageJ. White line illustrates example measurement of image intensity, and the intensity was plotted versus distance along this line (inset). The capillary width was calculated as the distance between two peak intensities in the intensity-distance plot (horizontal green line, inset). **B-F**. Example histograms of capillary size distributions in the stria vascularis of various animals. AIC calculations are shown for 1, 2, and 3 peaks in the distribution; the smallest AIC determines the number of peaks. Red curves show the best Gaussian fits to the determined number of peaks. Note the bimodal distribution of capillary widths for implanted animals in **C-D** and trimodal distributions in **E-F**.

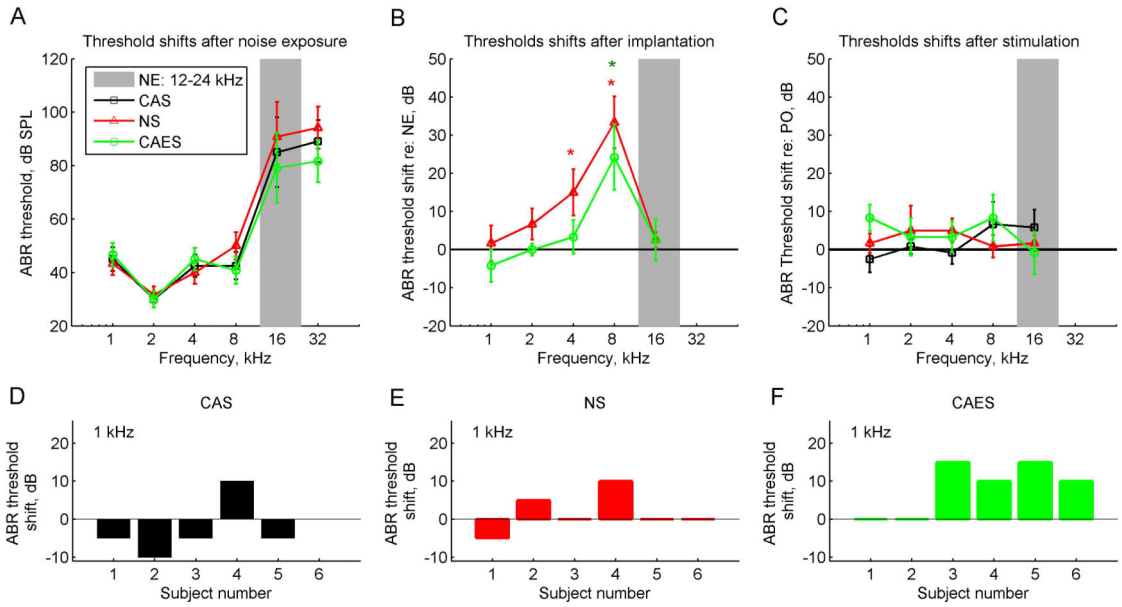

Figure 3.

Group-averaged ABR threshold changes due to noise exposure, implantation, and stimulation periods. Different symbols and colors represent the three subject groups; black squares represent the non-implanted CAS group, red triangles represent the implanted NS group, and green circles represent the implanted and stimulated CAES group. The gray bar indicates the frequency range of the noise exposure band (12-24 kHz). The vertical bars indicate standard deviations. **A.** ABR thresholds of the three groups after noise exposure. **B.** ABR threshold shifts of the implanted groups relative to the thresholds after noise exposure (NE) in A. Threshold shifts significantly greater than zero were seen for the NS group at 4 and 8 kHz, and for the CAES group at 8 kHz (asterisks; p=0.043, p=0.001, and p=0.045, respectively). **C.** ABR threshold shifts of the three groups at the conclusion of the study, i.e. after 9.5 weeks of electro-acoustic stimulation for the CAES group and the same time frame of acoustic-only and no stimulation for the CAS and NS groups, respectively. Threshold shifts are relative to post-operative (PO) thresholds. **D-F**. Distributions of threshold shifts at 1 kHz for the CAS, NS, and CAES groups, respectively.

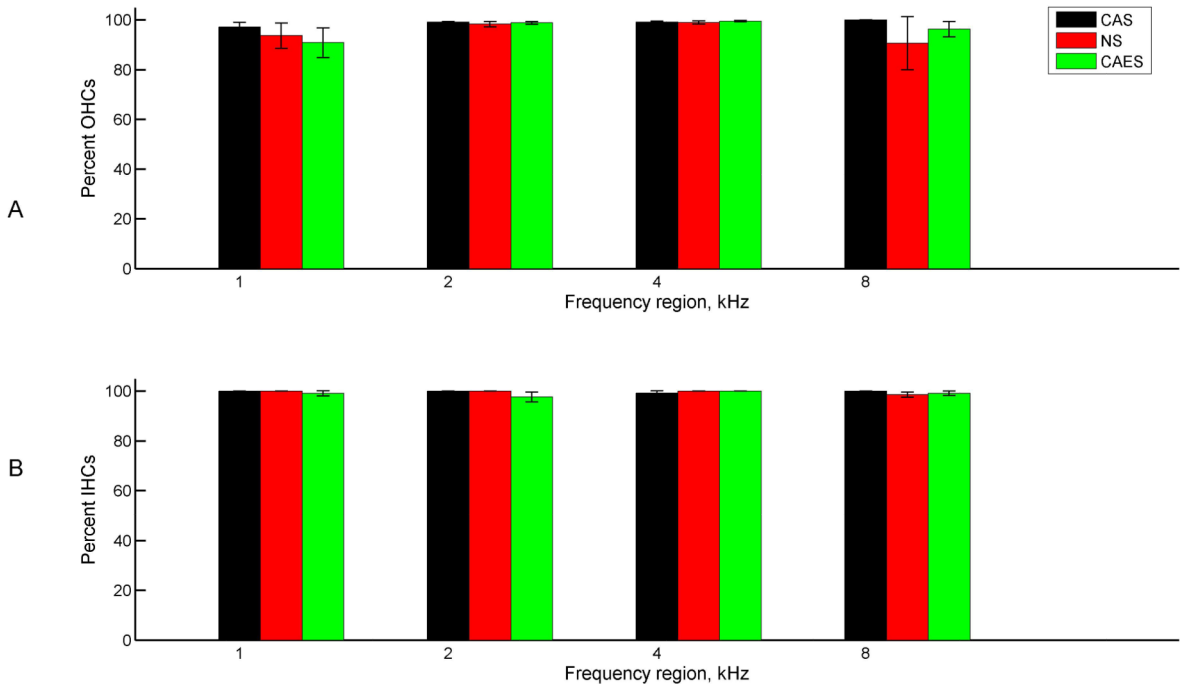

Figure 4.

Group-averaged hair cell survival percentages by frequency. Different colors represent the three groups as in Figure 3. **A.** Outer hair cells. **B.** Inner hair cells. No significant differences were observed between groups or across frequency.

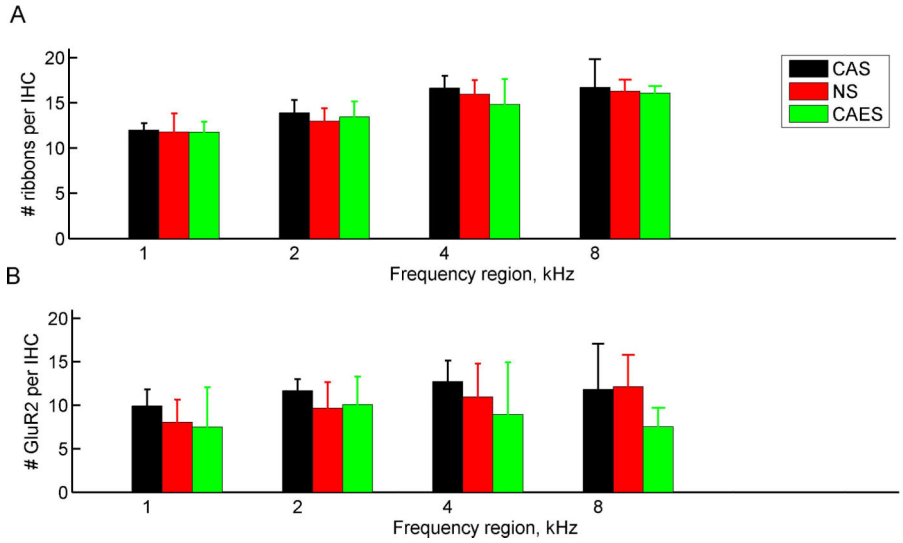

Figure 5.

Group-averaged presynaptic ribbon and post-synaptic receptor counts by frequency. Different colors represent the three groups as in Fig. 3. **A.** Presynaptic ribbon counts. Significant effects of group, but not frequency were observed ($p << 10^{-10}$, between/within subjects ANOVA). Post-hoc analyses revealed significant frequency differences for all groups between all frequency pairs except 4 and 8 kHz ($p < 0.05$, two-tailed t-test). **B.** Postsynaptic receptor counts. A significant effect of group, but not frequency, was observed ($p = 0.02$, between/within ANOVA). Vertical bars indicate standard deviations. (For interpretation of the references to color in this figure legend, the reader is referred to the web version of this article.)

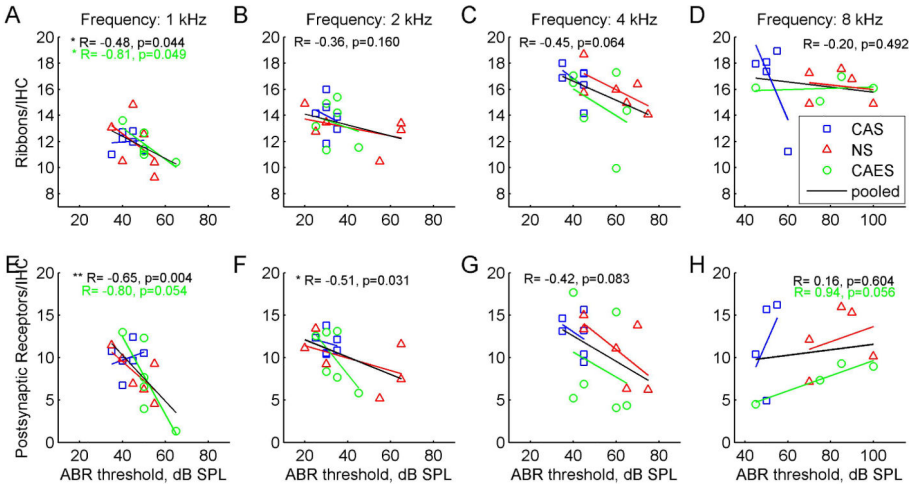

Figure 6.

Correlations of pre-synaptic ribbon and post-synaptic receptor counts with ABR thresholds by frequency. Different symbols and colors represent the three groups; blue squares represent the non-implanted CAS group, red triangles represent the implanted NS group, and green circles represent the implanted and stimulated CAES group. The corresponding colored lines represent linear fits to each group, and the black line represents the fit to the data pooled from all groups. Numbers at top of each figure indicate pooled correlation coefficients, and any individual group correlation coefficients with p-values <0.1. Note the shifted x-axis range for the 8 kHz correlations in D and H. **Top row or A-D**: ABR threshold-ribbon correlations for 1, 2, 4, and 8 kHz. Significant correlations were observed for the CAES group and for the pooled data at 1 kHz only ($p<0.05$, Pearson two-tailed correlation test). **Bottom row or E-H:** ABR threshold-post-synaptic receptor correlations for 1, 2, 4, and 8 kHz. Significant correlations were observed for the pooled data at 1 and 2 kHz ($p<0.05$, Pearson two-tailed correlation test). Note the larger y-axis range for the receptors compared to the ribbons in A-D.

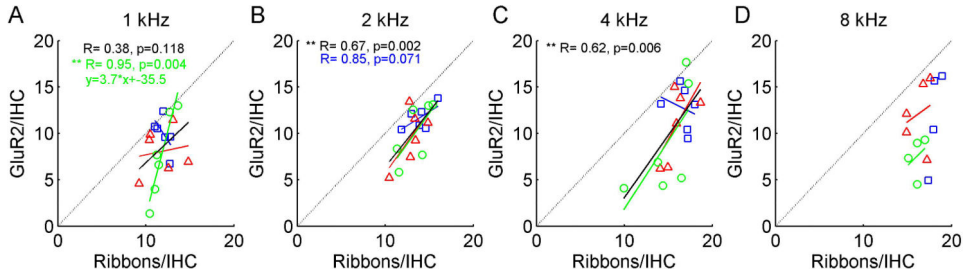

Figure 7.

Correlations of pre-synaptic ribbon versus post-synaptic receptor counts by frequency. Different symbols and colors represent the three groups as in Fig. 6. The corresponding colored lines represent linear fits to each group, and the black line represents the fit to the data pooled from all groups. Numbers at top of each figure indicate pooled correlation coefficients, and any individual group correlation coefficients with p-values <0.1. For reference, the dotted line indicates equality or a 1-1 relationship. **A-D**: ribbon-receptor count correlations for 1, 2, 4, and 8 kHz, respectively. Significant correlations were observed for the CAES group at 1 kHz and for pooled data at 2 kHz only ($p<0.05$, Pearson two-tailed correlation test). For the CAES group, the slope of the fit was 3.7, which means that there were 3.7 additional ribbons for every additional receptor. Note that for all frequencies and groups, receptor counts were generally below the dotted line relative to ribbon counts.

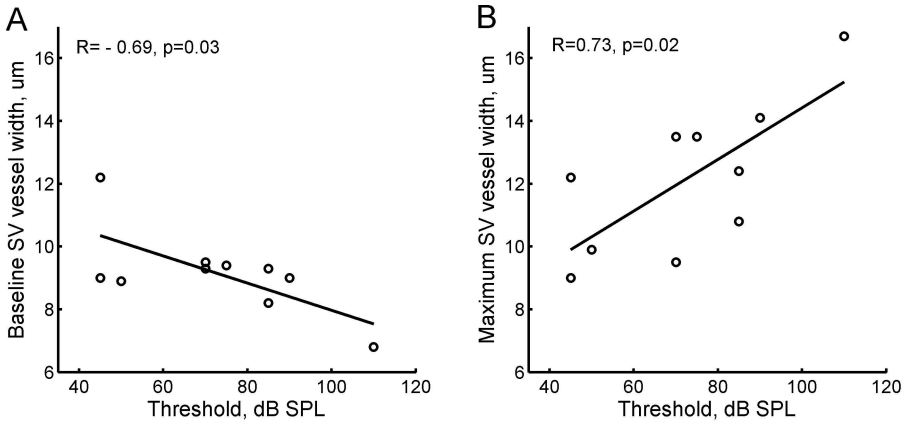

Figure 8.

Stria vascularis capillary widths at 6 kHz plotted versus acoustic thresholds at 8 kHz for individual animals in all groups. **A.** The minimum peak in the distributions of capillary widths, i.e. the first peak in Fig. 2B, versus threshold. A significant negative correlation (R= −0.69, p=0.03) was seen with threshold. **B.** The maximum peak in the distributions of capillary widths, i.e. the second peak in Fig. 2B when two peaks were present or the main peak when only one peak was present, versus threshold. A significant positive correlation (R=0.73, p=0.02) was seen with threshold.

Table 1

Inner and outer hair cell raw survival counts, total counts, and percent survival, by group and frequency region. Cochlear location corresponding to each frequency region is also given in parentheses below the frequency.

Group	Cell type	Frequency (Cochlear location from apex, in mm)	1 kHz (5.0)	2 kHz (7.2)	4 kHz (9.6)	8 kHz (12.1)
CAS	**Inner hair cells**	# Surviving	25.2	25.3	24.8	25.7
		Total	25.2	25.3	25	25.7
		% Survival	**100**	**100**	**99.2**	**100**
	Outer hair cells	# Surviving	92.8	93.5	92.2	95.0
		Total	95.6	94.3	93.0	95.0
		% Survival	**97.1**	**99.2**	**99.1**	**100.0**
NS	**Inner hair cells**	# Surviving	23.7	23.7	23.8	26.5
		Total	23.7	23.7	23.8	26.8
		% Survival	**100.0**	**100.0**	**100.0**	**98.9**
	Outer hair cells	# Surviving	88.7	89.3	89.7	97.7
		Total	94.0	90.8	90.5	107.2
		% Survival	**94.4**	**98.3**	**99.1**	**91.1**
CAES	**Inner hair cells**	# Surviving	22.7	22.8	22.8	27.2
		Total	22.9	23.3	22.8	27.4
		% Survival	**99.1**	**97.9**	**100.0**	**99.3**
	Outer hair cells	# Surviving	85.8	87.3	80.8	98.3
		Total	92.6	88.5	81.3	101.8
		% Survival	**92.7**	**98.6**	**99.4**	**96.6**